Inorganic Chemistry

ARTICLE

pubs.acs.org/IC

New Quaternary Tellurite and Selenite: Synthesis, Structure, and Characterization of Centrosymmetric $InVTe_2O_8$ and Noncentrosymmetric $InVSe_2O_8$

Dong Woo Lee,[†] Seung-Jin Oh,[†] P. Shiv Halasyamani,[‡] and Kang Min Ok*[,†]

[†]Department of Chemistry, Chung-Ang University, 221 Heukseok-dong, Dongjak-gu, Seoul 156-756, Republic of Korea

[‡]Department of Chemistry, University of Houston, 136 Fleming Building, Houston, Texas 77204-5003, United States

Supporting Information

ABSTRACT: Two new quaternary mixed metal oxide materials—$InVTe_2O_8$ and $InVSe_2O_8$—have been synthesized, as crystals and pure bulk powders by standard solid-state reactions using In_2O_3, V_2O_5, and TeO_2 (or SeO_2) as reagents. The crystal structures of the reported materials were determined using single-crystal X-ray diffraction. $InVTe_2O_8$ crystallizes in the monoclinic centrosymmetric space group $P2_1/n$ (No. 14), with unit-cell parameters of a = 7.8967(16) Å, b = 5.1388(10) Å, c = 16.711(3) Å, β = 94.22(3)°, and Z = 4, and $InVSe_2O_8$ crystallizes in the noncentrosymmetric space group Pm (No. 6) with unit-cell parameters of a = 4.6348(9) Å, b = 6.9111(14) Å, c = 10.507(2) Å, β = 97.77(3)°, and Z = 2. While the centrosymmetric $InVTe_2O_8$ shows a two-dimensional (2D) layered structure composed of InO_6 octahedra, VO_4 tetrahedra, and TeO_4 polyhedra, the noncentrosymmetric $InVSe_2O_8$ exhibits a three-dimensional (3D) framework structure with distorted InO_6 octahedra, VO_5 square pyramids, and SeO_3 polyhedra. Powder second-harmonic generation (SHG) measurements on $InVSe_2O_8$, using 1064-nm radiation, indicate that the material has a SHG efficiency ~30 times that of α-SiO_2. Additional SHG measurements reveal that the material is not phase-matchable (Type 1). Infrared, ultraviolet−visible light (UV−vis) diffuse reflectance, and thermogravimetric analyses for the two compounds are also presented, as are dipole moment calculations.

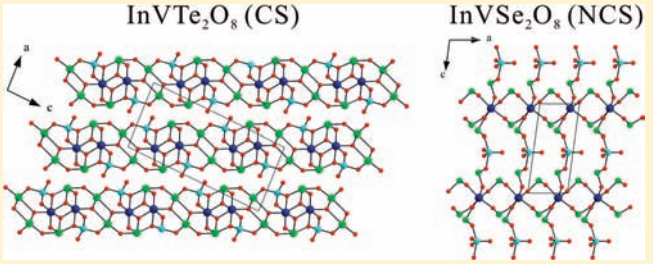

INTRODUCTION

Both tellurium dioxide (TeO_2) and selenium dioxide (SeO_2) have been used widely in the syntheses of a variety of new solid-state materials, because of their lower melting and triple points (733 °C for TeO_2, 340 °C for SeO_2), respectively. These accessible temperatures have enabled them to be used as fluxes for crystal growth.[1−4] In addition, the excellent reactivities of TeO_2 and SeO_2 have enabled them to be used in the formation of many new oxide materials.[5−9] The variable coordination environments of the Te^{4+} and Se^{4+} cations have also been of particular interest. Specifically, the Te^{4+} cation can exhibit a variety of structural motifs such as a trigonal pyramid, seesaw, and square pyramid.[10−13] If the various coordination geometries are combined with other polyhedral moieties, a great deal of framework architecture flexibility is possible. Finally, the Se^{4+} and Te^{4+} cations inherently possess asymmetric structural geometry attributable to the nonbonded electron pair. Materials containing lone-pair cations have been shown to exhibit local noncentrosymmetric coordination environments.[14−16] Many strategies have been suggested to increase the incidence of crystallographic noncentrosymmetry in any new material.[17−20] Noncentrosymmetric (NCS) materials are of topical and technological interest, because of their second harmonic generation (SHG), piezoelectric, ferroelectric, and pyroelectric properties.[21−24] With oxide materials, the NCS structures are often observed in materials that contain second-order Jahn−Teller (SOJT) distortive cations,[25−28] i.e., octahedrally coordinated d^0 transition-metal ions (Ti^{4+}, V^{5+}, W^{6+}, etc.) and lone-pair cations (Se^{4+}, Te^{4+}, I^{5+}, etc.). With the d^0 metal cations, a distortion from the center of their oxide octahedron toward a corner, edge, or face is often observed,[29] whereas, with the lone-pair cations, a nonbonded electron pair is found.[30−32] Since the asymmetric environments are one of the major factors that substantially influence the materials' NCS properties, understanding the structural basis of the local site symmetry is very important. However, the local asymmetric environment is a necessary, but not sufficient, condition for creating macroscopic NCS. In other words, the material may crystallize with the asymmetric units aligned antiparallel, leading to macroscopic centrosymmetry. Thus, to understand the factors that determine overall crystallographic centrosymmetry, it is important to appreciate and understand the local asymmetry as well as the macroscopic symmetry. As such, the rational design of NCS materials remains an ongoing challenge. We have chosen to investigate the In^{3+}−V^{5+}−Te^{4+} (Se^{4+})−oxide system. Several quaternary oxide materials in the M^{n+}−V^{5+}−Te^{4+}−oxide[33−42] or M^{n+}−V^{5+}−Se^{4+}−oxide systems have been reported.[43−47] We were very interested in introducing a p-element (i.e., In^{3+}) that can

Received: January 20, 2011
Published: April 12, 2011

Table 1. Crystallographic Data for $InVTe_2O_8$ and $InVSe_2O_8$

formula	$InVTe_2O_8$	$InVSe_2O_8$
fw	548.96	451.68
space group	$P2_1/n$ (No. 14)	Pm (No. 6)
a (Å)	7.8967(16)	4.6348(9)
b (Å)	5.1388(10)	6.9111(14)
c (Å)	16.711(3)	10.507(2)
β (°)	94.22(3)	97.77(3)
V (Å^3)	676.3(2)	333.48(11)
Z	4	2
T (°C)	200.0(2)	200.0(2)
λ (Å)	0.71073	0.71073
ρ_{calcd} (g cm^{-3})	5.391	4.498
μ (mm^{-1})	13.254	15.779
$R(F)^a$	0.0286	0.0343
$R_w(F_o^2)^b$	0.0680	0.0589

$^a R(F) = \Sigma||F_o| - |F_c||/\Sigma|F_o|$. $^b R_w(F_o^2) = [\Sigma w(F_o^2 - F_c^2)^2/\Sigma w(F_o^2)^2]^{1/2}$.

form a larger and stable octahedral environment with very interesting structural features. In fact, the longer In−O bonds in NCS $In_2(Se_2O_5)_3$, compared to the Ga−O and Al−O bonds in CS $Al_2(Se_2O_5)_3$ and $Ga_2(Se_2O_5)_3$, respectively, provided greater flexibility, which, in turn, easily relates the asymmetric moiety in the structure.[3] Here, we report the synthesis, structural determinations, and complete characterizations of two new quaternary oxide materials: $InVTe_2O_8$ and $InVSe_2O_8$. To the best of our knowledge, the reported materials are the first examples in the In^{3+}−V^{5+}−Te^{4+} (Se^{4+})−oxide family. With the NCS oxide, $InVSe_2O_8$, detailed SHG properties will also be reported.

EXPERIMENTAL SECTION

Reagents. In_2O_3 (Alfa Aesar, 99.9%), V_2O_5 (Aldrich, 98%), TeO_2 (Alfa Aesar, 99.9%), and SeO_2 (Aldrich, 98%) were used as received.

Synthesis. Crystals of $InVTe_2O_8$ and $InVSe_2O_8$ were prepared by standard solid-state reactions. In_2O_3 (0.228 g (1.00×10^{-3} mol)), V_2O_5 (0.182 g (1.00×10^{-3} mol)), and SeO_2 (0.444 g (4.00×10^{-3} mol)) or TeO_2 (0.638 g (4.00×10^{-3} mol)) was thoroughly mixed with an agate mortar and pestle, under an atmosphere of dry argon. The respective reaction mixtures were introduced into fused-silica tubes that were evacuated and subsequently sealed. Each tube was gradually heated to 250 °C for 5 h, and then to 550 °C for 48 h (700 °C for 48 h for $InVTe_2O_8$). The samples were cooled at a rate of 1 °C h^{-1} to room temperature. The products contained light brown and light green crystals for $InVTe_2O_8$ and $InVSe_2O_8$, respectively. Pure polycrystalline samples of $InVTe_2O_8$ and $InVSe_2O_8$ were obtained through similar solid-state reactions. However, the reaction temperatures have been reduced and several intermittent regrindings have been applied; each reaction mixture within a sealed fused-silica tube was gradually heated to 250, 350, 400, and 440 °C for 12 h (600 °C for $InVTe_2O_8$) at each temperature with intermediate regrindings. The powder X-ray diffraction (XRD) patterns on the resultant polycrystalline products exhibited materials that were single phase and were in good agreement with the generated patterns from the single-crystal data (see the Supporting Information).

Single-Crystal X-ray Diffraction. The structures of $InVTe_2O_8$ and $InVSe_2O_8$ were determined by standard crystallographic methods. A light-brown plate (0.04 mm × 0.08 mm × 0.24 mm) for $InVTe_2O_8$ and a light green plate (0.04 mm × 0.06 mm × 0.20 mm) for $InVSe_2O_8$ were used for single-crystal data analyses. All of the data were collected using a Bruker SMART APEX diffractometer that was equipped with a 1K CCD area detector, using graphite-monochromated Mo Kα radiation at 200 K at the Korea Basic Science Institute. A hemisphere of data was collected using a narrow-frame method with scan widths of 0.30° in omega, and an exposure time of 5 s/frame. The first 50 frames were remeasured at the end of the data collection to monitor instrument and crystal stability. The maximum correction applied to the intensities was <1%. The data were integrated using the SAINT program,[48] with the intensities corrected for Lorentz factor, polarization, air absorption, and absorption attributable to the variation in the path length through the detector faceplate. A semiempirical absorption correction was made on the hemisphere of data with the SADABS program.[49] The data were solved and refined using SHELXS-97 and SHELXL-97, respectively.[50,51] All of the metal atoms were refined with anisotropic thermal parameters and converged for $I > 2\sigma(I)$. All calculations were performed using the WinGX-98 crystallographic software package.[52] Crystallographic data and selected bond distances for the reported material are given in Tables 1 and 2.

Table 2. Selected Bond Distances for $InVTe_2O_8$ and $InVSe_2O_8$

$InVTe_2O_8$		$InVSe_2O_8$	
bond	bond distance (Å)	bond	bond distance (Å)
In(1)−O(1)	2.062(9)	In(1)−O(1)	2.100(10)
In(1)−O(2)	2.124(9)	In(1)−O(2)	2.198(9)
In(1)−O(3)	2.197(9)	In(1)−O(3)	2.113(10)
In(1)−O(4)	2.155(9)	In(1)−O(4)	2.199(9)
In(1)−O(4)	2.183(9)	In(1)−O(5)	2.187(10)
In(1)−O(5)	2.178(9)	In(1)−O(6)	2.179(9)
V(1)−O(3)	1.816(9)	V(1)−O(7)	1.936(13)
V(1)−O(5)	1.685(10)	V(1)−O(8)	1.846(6)
V(1)−O(7)	1.830(9)	V(1)−O(9)	1.587(11)
V(1)−O(8)	1.615(9)	V(1)−O(10)	1.947(13)
Te(1)−O(1)	1.856(9)	V(1)−O(11)	1.842(6)
Te(1)−O(3)	2.131(8)	Se(1)−O(1) × 2	1.691(11)
Te(1)−O(4)	1.928(9)	Se(1)−O(5)	1.735(15)
Te(1)−O(6)	2.103(9)	Se(2)−O(2)	1.746(15)
Te(2)−O(2)	1.874(9)	Se(2)−O(3) × 2	1.677(10)
Te(2)−O(2)	2.506(9)	Se(3)−O(6)	1.728(15)
Te(2)−O(6)	1.907(9)	Se(3)−O(7) × 2	1.690(12)
Te(2)−O(7)	1.905(9)	Se(4)−O(4)	1.738(15)
		Se(4)−O(10) × 2	1.696(11)

Powder X-ray Diffraction. Powder XRD was used to confirm the phase purity for the synthesized material. The powder XRD data were collected on a Scintag XDS2000 diffractometer, at room temperature (Cu Kα radiation, $\theta-\theta$ mode, flat-plate geometry), equipped with a Peltier germanium solid-state detector in the 2θ range of 5°−70°, with a step size of 0.02° and a step time of 1 s. The experimental powder XRD patterns for both materials are in good agreement with those calculated data from the single-crystal models.

Infrared Spectroscopy. Infrared spectra were recorded on a Varian Model 1000 FT-IR spectrometer in the 400−4000 cm^{-1} range, with the sample embedded in a KBr matrix.

UV−vis Diffuse Reflectance Spectroscopy. Ultraviolet−visible (UV-vis) reflectance data were collected on a Varian Cary 500 scan UV−vis−NIR spectrophotometer over a spectral range of 200−1500 nm at room temperature. Poly(tetrafluoroethylene) was used as a reference material. Reflectance spectra were converted to absorbance data, using the Kubelka−Munk function.[53,54]

Thermogravimetric Analysis. Thermogravimetric analysis was performed on a Setaram LABSYS TG-DTA/DSC thermogravimetric analyzer. The polycrystalline samples of $InVTe_2O_8$ and $InVSe_2O_8$ were

dx.doi.org/10.1021/ic200135k |Inorg. Chem. 2011, 50, 4473–4480

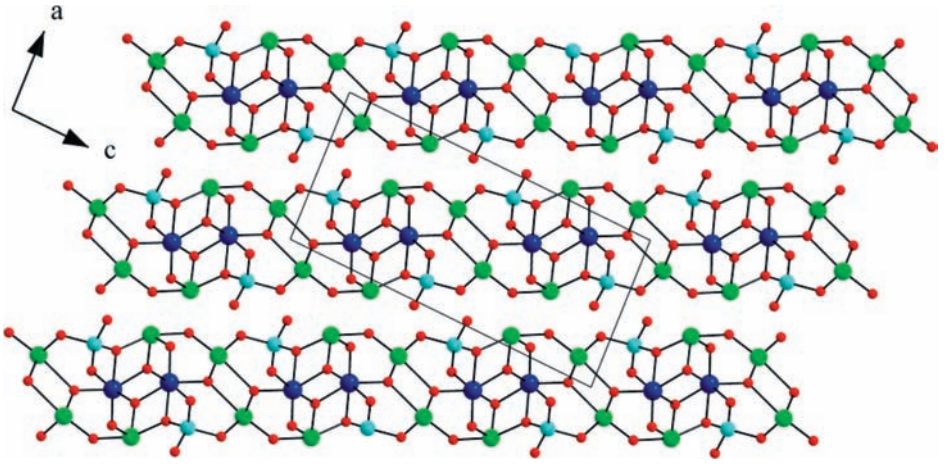

Figure 1. Ball-and-stick representation of $InVTe_2O_8$ in the *ac*-plane. The distorted InO_6 octahedra, VO_4 tetrahedra, and asymmetric TeO_4 polyhedra link to form a two-dimensional (2D) layered crystal structure (blue, In; cyan, V; green, Te; red, O).

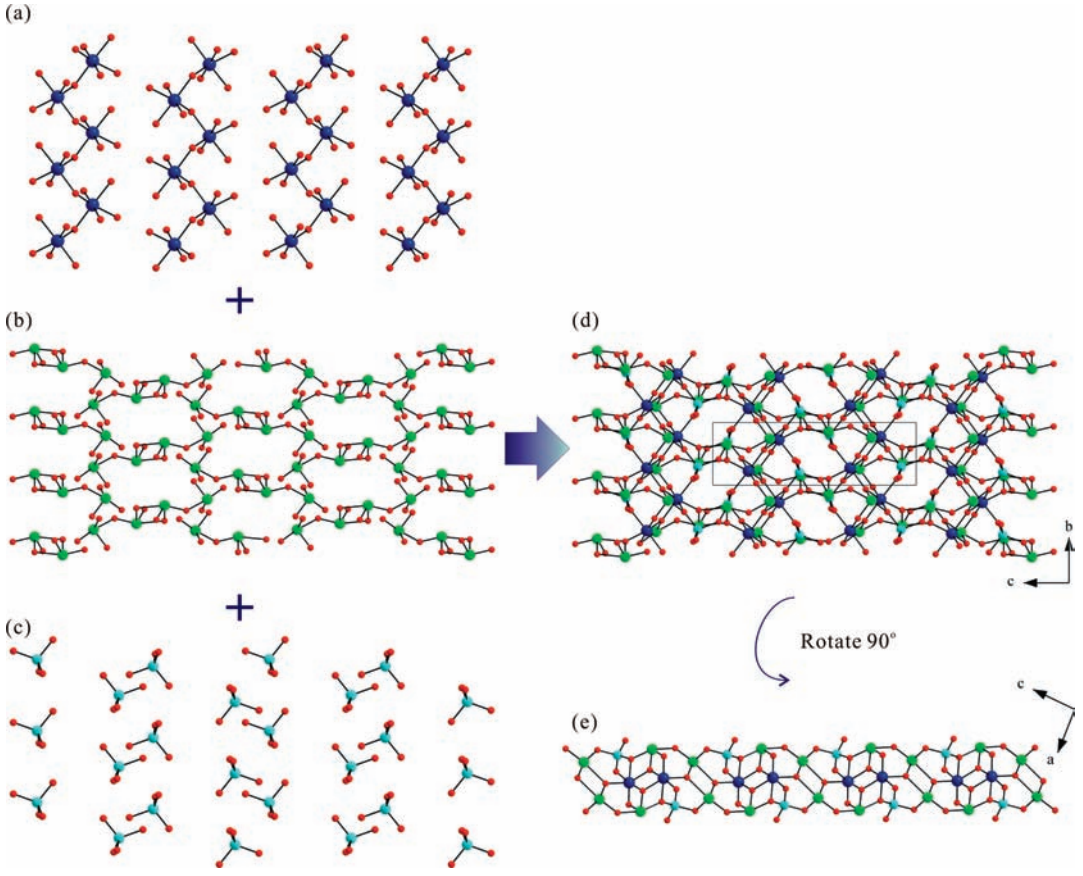

Figure 2. Ball-and-stick diagrams representing (a) InO_6 chains along the [010] direction, (b) Te_4O_{12} tetramers, (c) VO_4 tetrahedra, and the "linking" of the polyhedra to form a 2D layer structure of $InVTe_2O_8$ in the (d) *bc*-plane and (e) *ac*-plane (blue, In; cyan, V; green, Te; red, O).

contained within alumina crucibles and heated at a rate of 10 °C min^{-1} from room temperature to 800 °C under flowing argon.

Scanning Electron Microscope/Energy-Dispersive Analysis by X-ray (SEM/EDAX). SEM/EDAX analysis has been performed using a Hitachi Model S-3400N/Horiba Energy Model EX-250 system. EDAX for $InVTe_2O_8$ and $InVSe_2O_8$ reveal In:V:Te and In:V:Se ratios of ~1:1:2.

Second-Order Nonlinear Optical Measurements. Powder SHG measurements on polycrystalline $InVSe_2O_8$ were performed on a modified Kurtz-NLO system,[55] using 1064-nm radiation. A detailed description of the equipment and the methodology used has been published.[56] The SHG efficiency has been shown to be strongly dependent on particle size; therefore, polycrystalline samples were ground and sieved to distinct particle size ranges (20−45 μm, 45−63 μm, 63−75 μm, 75−90 μm, and >90 μm). To make relevant comparisons with known SHG materials, crystalline α-SiO_2 and $LiNbO_3$ were also ground and sieved into the same particle size

dx.doi.org/10.1021/ic200135k |*Inorg. Chem.* 2011, 50, 4473–4480

ranges. Powders with a particle size of 45−63 μm were used to compare the SHG intensities. No index matching fluid was used in any of the experiments.

RESULTS AND DISCUSSION

$InVTe_2O_8$. $InVTe_2O_8$ is a new quaternary $In^{3+}-V^{5+}-Te^{4+}-$oxide material that crystallizes in centrosymmetric space group $P2_1/n$ (No. 14). The material exhibits a two-dimensional (2D) layered crystal structure consisting of InO_6 octahedra, VO_4 tetrahedra, and asymmetric TeO_4 polyhedra (see Figure 1). Each In^{3+} cation is bound to six oxygen atoms in a slightly distorted octahedral environment, with bond lengths ranging from 2.062(9) Å to 2.197(9) Å. The O−In−O bond angles range from 72.6(3)° to 176.7(3)°. The unique V^{5+} cation is in a distorted tetrahedral environment with two "short" V−O distances (1.615(9) and 1.685(10) Å) and two "normal" V−O distances (1.816(9) and 1.830(9) Å). The O−V−O bond angles range from 107.3(5)° to 111.9(4)°. There are two unique Te^{4+} cations that are bonded to four oxygen atoms. The $Te(1)^{4+}$ cations exhibit two slightly shorter (1.856(9) and 1.928(9) Å) and two slightly longer Te−O (2.103(9) and 2.131(8) Å) bond distances in a distorted seesaw environment. However, the $Te(2)^{4+}$ cations show three shorter bond lengths (1.874(9) and 1.907(9) Å) and one very long Te−O (2.506(9) Å) bond length. The Te^{4+} cations are in a highly asymmetric coordination environment, which is attributable to their lone pairs. The O−Te−O bond angles range from 70.0(4)° to 160.7(3)°. A list of the selected bond distances is given in Table 2. The bond distances are consistent with those previously reported.[8,9,44] In connectivity terms, the structure may be written as a neutral framework of

$$\left\{ \left[InO_{2/3}O_{4/3}\right]^{-1.667} \quad \left[VO_{2/2}O_{1/3}O_{1/1}\right]^{+0.333} \quad 2\left[TeO_{2/2}O_{2/3}\right]^{+0.667} \right\}^{0}$$

Bond valence calculations[57,58] on $InVTe_2O_8$ result in values of 3.08, 4.96, and 4.02−4.03 for In^{3+}, V^{5+}, and Te^{4+}, respectively. Zig-zag chains of InO_6 corner-shared octahedra are observed along the [010] direction (see Figure 2a). The two $Te(1)O_4$ and $Te(2)O_4$ polyhedra are also corner-shared forming Te_2O_7 "dimers" (see Figure 2b) that are linked to form a tetrameric Te_4O_{12} unit (see Figure 2b). Finally, the InO_6 zigzag chains, the Te_4O_{12} tetramers, and the VO_4 tetrahedra link together and form the novel 2D layered structure (see Figure 2).

$InVSe_2O_8$. $InVSe_2O_8$ is another new quaternary mixed metal oxide material with an $In^{3+}-V^{5+}-Se^{4+}-$oxide composition that crystallizes in noncentrosymmetric polar space group Pm (No. 6). The structure contains distorted InO_6 octahedra, VO_5 square pyramids, and asymmetric SeO_3 polyhedra (see Figure 3). There is a unique In^{3+} cation in a distorted octahedral environment, bound to six oxygen atoms. The In−O bond lengths range from 2.100(10) Å to 2.199(9) Å. The O−In−O bond angles range from 74.5(4)° to 170.6(5)°. Each V^{5+} is bound to five oxygen atoms in a slightly distorted square pyramidal environment with one "short" (1.587(11) Å) and four "normal" V−O distances (1.842(6)−1.947(13) Å). The O−V−O bond angles range from 85.8(6)° to 155.7(5)°. The four unique Se^{4+} cations ($Se(1)^{4+}-Se(4)^{4+}$) are bound to three oxygen atoms. All of the Se^{4+} cations are in a highly asymmetric coordination environment, which is attributed to their nonbonded electron pairs. The Se−O bond distances range from 1.677(10) to 1.746(15) Å. The O−Se−O bond angles range from 96.2(5)° to 108.4(8)°. A list of the selected bond distances is given in Table 2. The bond distances are consistent with those previously reported.[3,59,60] In

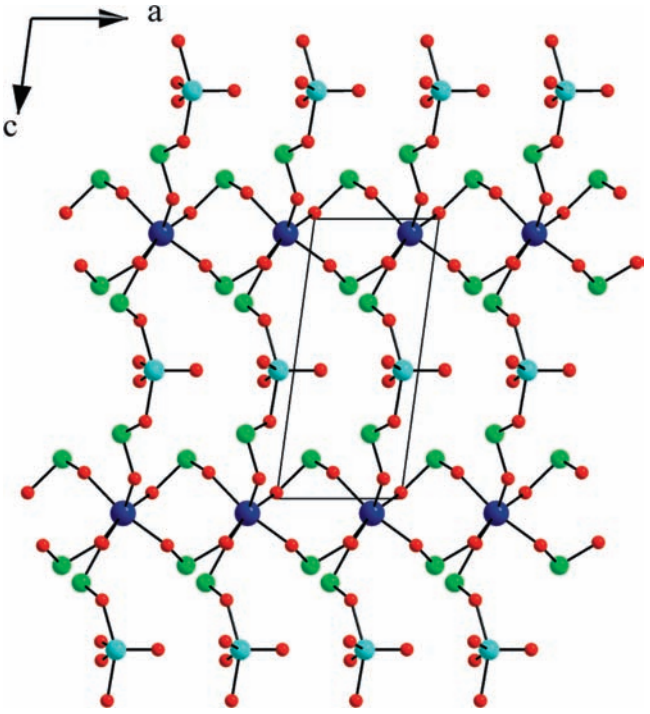

Figure 3. Ball-and-stick model of $InVSe_2O_8$ in the *ac*-plane (blue, In; cyan, V; green, Se; red, O). The distorted InO_6 octahedra, VO_5 square pyramids, and asymmetric SeO_3 polyhedra link to form a three-dimensional (3D) framework structure.

connectivity terms, the structure may be written as a neutral framework of

$$\left\{ \left[InO_{2/3}O_{4/3}\right]^{-1.667} \quad \left[VO_{4/2}O_{1/1}\right]^{-1} \quad 2\left[SeO_{2/2}O_{1/3}\right]^{+1.333} \right\}^{0}$$

Bond valence calculations[57,58] on $InVSe_2O_8$ result in 2.97, 5.09, and 4.06−4.13 for In^{3+}, V^{5+}, and Se^{4+}, respectively. Similar to $InVTe_2O_8$, the chains of InO_6 octahedra are observed running along the [010] direction; however, in $InVSe_2O_8$, the InO_6 octahedra are edge-shared (see Figure 4a). The VO_5 square pyramids are corner-shared, creating infinite chains running along the [010] direction (see Figure 4b). Interestingly, all the apical V═O bonds in the VO_5 square pyramids are pointing toward the [100] direction within the chains. The InO_6 chains, the VO_5 chains, and SeO_3 groups are linked together and form a novel three-dimensional (3D) framework structure (see Figure 4). In $InVSe_2O_8$, the SeO_3 groups serve as intrachain and interchain linkers.

Infrared Spectroscopy. In−O, V−O, Te−O, and Se−O vibrations were observed in the infrared spectra. The In−O vibrations are observed at ∼405−429 cm^{-1}. The bands occurring at ∼948−974 and ∼701−866 cm^{-1} can be assigned to V═O (short terminal V−O bonds) and V−O vibrations, respectively. The stretches at 547−788 and 459−823 cm^{-1} can be attributed to Te−O and Se−O vibrations, respectively. The infrared vibrations and assignments are listed in Table 3. The assignments are consistent with those previously reported.[3,59,61−64]

UV−vis Diffuse Reflectance Spectroscopy. The UV−vis diffuse reflectance spectra for $InVTe_2O_8$ and $InVSe_2O_8$ have been deposited in the Supporting Information. $InVTe_2O_8$ is light brown, whereas $InVSe_2O_8$ is light green. These spectra show that the absorption is ∼2.1−2.8 eV. Absorption (K/S) data were

dx.doi.org/10.1021/ic200135k |*Inorg. Chem.* 2011, 50, 4473–4480

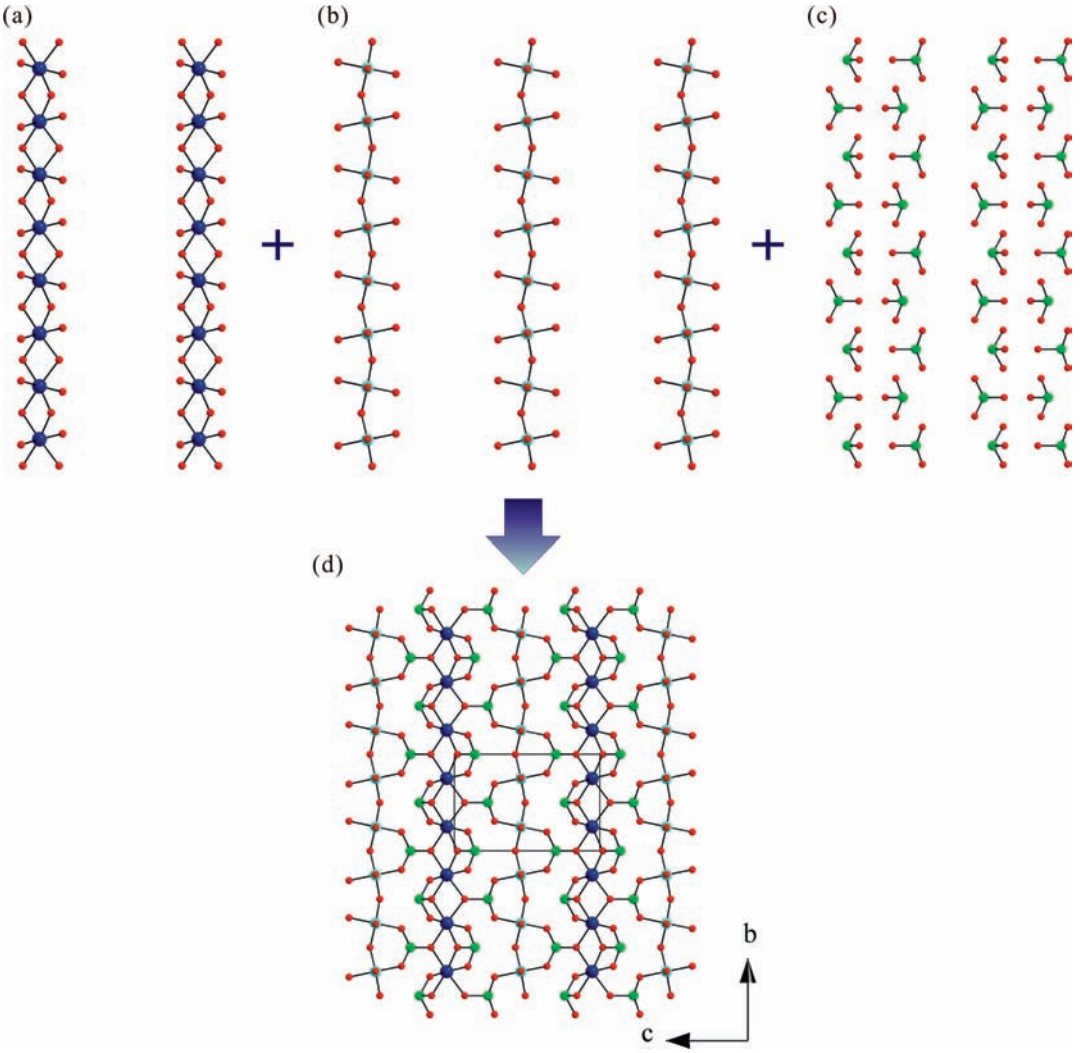

Figure 4. Ball-and-stick models representing (a) InO_6 chains running along the [010] direction, (b) VO_5 chains running along the [010] direction, (c) SeO_3 polyhedra, and (d) the "linking" of the polyhedra to form a 3D framework structure of $InVSe_2O_8$ in the *bc*-plane (blue, In; cyan, V; green, Se; red, O).

calculated from the following Kubelka–Munk function:[53,54]

$$F(R) = \frac{(1-R)^2}{2R} = \frac{K}{S}$$

where R is the reflectance, K the absorption, and S the scattering. In the (K/S)-vs-E plot, extrapolating the linear part of the rising curve to zero provided the onset of absorption at 2.8 and 2.1 eV for $InVTe_2O_8$ and $InVSe_2O_8$, respectively. It is likely that the visible absorption in the reported compounds can be attributed to charge transfer in the vanadyl units. The onset of absorption values for the reported compounds is in good agreement with the previous study of compounds that contained VO_2^+ vanadyl units.[63,65]

Thermogravimetric Analysis. The thermal behaviors of $InVTe_2O_8$ and $InVSe_2O_8$ were investigated using thermogravimetric analysis (TGA). As indicated by the TGA diagram, $InVTe_2O_8$ is stable up to 800 °C. No weight loss was observed. However, $InVSe_2O_8$ was only stable up to 450 °C. Above this temperature, decomposition occurs, which is attributable to the sublimation of SeO_2. Powder XRD measurement on the calcined material under an argon atmosphere revealed that $InVSe_2O_8$ decomposes to $InVO_4$[66] and In_2VO_5.[67] The TGA plots for both materials are shown in the Supporting Information.

Second-Order Nonlinear Optical Measurements. Since $InVSe_2O_8$ crystallizes in a noncentrosymmetric space group, we investigated its nonlinear optical properties. Powder SHG measurements, using 1064-nm radiation, indicated that $InVSe_2O_8$ has a SHG efficiency ~30 times that of α-SiO_2. By sieving $InVSe_2O_8$ powder into various particle sizes, ranging from 20 μm to 150 μm, and by measuring the SHG as a function of particle size, we were able to determine the Type 1 phase-matching capabilities of the material. As seen in Figure 5, $InVSe_2O_8$ is not phase-matchable. Based on the SHG efficiency and phase-matching measurements, $InVSe_2O_8$ falls into the Class C category of SHG materials, as defined by Kurtz and Perry.[55] Once the SHG efficiency and the phase-matching capability of a material are known, the bulk SHG efficiency ($\langle d_{eff}\rangle_{exp}$) can be estimated.[68] For $InVSe_2O_8$, $\langle d_{eff}\rangle_{exp} \approx 3.0$ pm V^{-1}.

Structure–Property Relationships. The SHG response can be understood by examining the polarization of the asymmetric polyhedra, since macroscopic NCS is usually observed when locally polar asymmetric coordination polyhedra add constructively. Thus, determining the "net" direction of the polarizations enables us to understand the origin and magnitude of the SHG properties. We assume that the InO_6 octahedra do not contribute

dx.doi.org/10.1021/ic200135k |*Inorg. Chem.* 2011, 50, 4473–4480

Table 3. Infrared Vibrations (cm^{-1}) for $InVTe_2O_8$ and $InVSe_2O_8$

$InVTe_2O_8$			
In−O	V═O	V−O	Te−O
405	948	510	547
		863	701
			788
$InVSe_2O_8$			
In−O	V═O	V−O	Se−O
429	974	510	459
		866	665
			795
			823

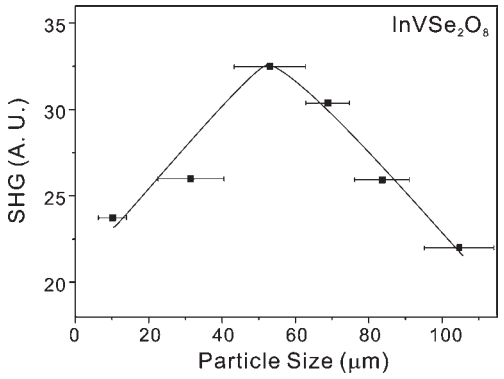

Figure 5. Phase-matching curve (Type 1) for $InVSe_2O_8$. The curve is drawn to guide the eye, and is not a fit to the data.

significantly toward the SHG efficiency, since the In^{3+} is not a SOJT distortive cation. For the V^{5+} cations, each VO_5 square pyramid unit is aligned toward one direction. More specifically, all the apical V═O bonds for the VO_5 square pyramids are directed toward the [100] direction (see Figure 6); since the local moment for the VO_5 square pyramids is in the opposite direction of the V═O bond, a net moment is observed pointing in the $[\bar{1}00]$ direction. Each SeO_3 unit also has a dipole moment that is attributable to the different charge distribution on Se and O atoms, as well as the asymmetric environment arising from the alignment of lone pairs. The lone pairs on the asymmetric cations $Se(1)^{4+}$ and $Se(2)^{4+}$ approximately point toward the [001] and $[00\bar{1}]$ directions, respectively; thus, the polarizations associated with $Se(1)^{4+}$ and $Se(2)^{4+}$ cancel. The lone pairs attached on $Se(3)^{4+}$ and $Se(4)^{4+}$ point approximately parallel toward the $[\bar{1}00]$ direction (see Figure 6). The local moment for the SeO_3 points in the opposite direction of the lone pair. Thus, the net effect of this alignment of lone pairs on Se^{4+} cations is a larger moment in the [100] direction. One can also notice that the moments for VO_5 square pyramids and SeO_3 are pointed in opposite directions. Taking the moments as a whole, a net moment is observed along the $[\bar{1}00]$ direction. As we will discuss later, the local dipole moment calculations indicate that the moment for VO_5 square pyramid is larger than that of the SeO_3 group. Our SHG measurements show the relatively weak SHG efficiency (~30 times that of α-SiO_2), which we suggest is

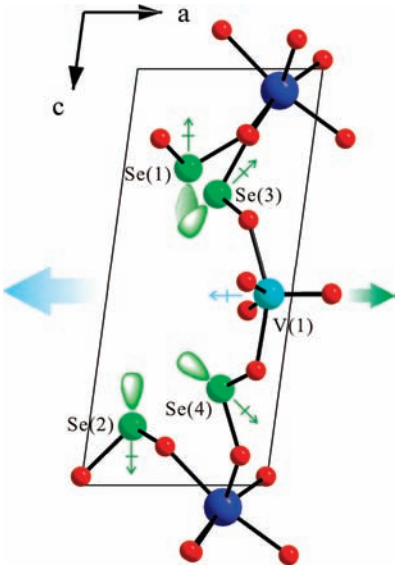

Figure 6. Ball-and-stick representation of $InVSe_2O_8$ (blue, In; cyan, V; green, Se; red, O). A moment is observed toward the $[\bar{1}00]$ direction, which is attributable to the alignment of the VO_5 square pyramids. Also, a larger net moment attributed to the sum of the asymmetric environment, which is attributable to the alignment of lone pairs on Se^{4+} cations, is observed in the [100] direction. Once taken as a whole, a net moment is observed along the $[\bar{1}00]$ direction.

attributable to the lack of greater constructive addition of the dipole moments. We believe that the SHG light (532 nm) may also be underestimated, which is attributable to the light green color of $InVSe_2O_8$.

In order to better understand the asymmetric coordination environment, we also calculated the local dipole moment for Te^{4+} and Se^{4+} in $InVTe_2O_8$ and $InVSe_2O_8$. This approach has been described earlier, with respect to metal oxyfluoride octahedra.[69,70] We found that the local dipole moments for the two unique TeO_4 polyhedra—$Te(1)O_4$ and $Te(2)O_4$—in $InVTe_2O_8$ are ~9.08 D and ~6.87 D, respectively. [Here, D represents Debyes.] Also, the local dipole moments for the four SeO_3 polyhedra in $InVSe_2O_8$ exhibit very similar values that range from 7.09 D to 7.87 D. The dipole moments for $Se(1)O_3$, $Se(2)O_3$, $Se(3)O_3$, and $Se(4)O_3$ were calculated to be 7.43, 7.09, 7.87, and 7.50 D, respectively. The values are consistent with those recently reported dipole moments for TeO_4 and SeO_3 polyhedra.[60,71] The local dipole moment for the VO_5 group can be calculated to be 28.19 D, using the same calculation method.

CONCLUSIONS

We have successfully synthesized two new quaternary mixed metal oxide materials—$InVTe_2O_8$ and $InVSe_2O_8$—by standard solid-state reactions. Although the materials are stoichiometrically equivalent, crystallographic data indicate that $InVTe_2O_8$ is centrosymmetric with a two-dimensional (2D) layered structure, whereas $InVSe_2O_8$ is noncentrosymmetric (NCS) with a three-dimensional (3D) framework structure. Powder second-harmonic generation (SHG) measurements on $InVSe_2O_8$, using 1064-nm radiation, indicate that the material is not phase-matchable (Type 1), with a SHG efficiency ~30 times that of α-SiO_2. Full spectroscopic characterizations, thermal analysis, and dipole moment have been performed on the reported materials. The combination of cations

dx.doi.org/10.1021/ic200135k |*Inorg. Chem.* 2011, 50, 4473–4480

with greater flexibility and asymmetric polyhedra may be the driving force for the crystallization of a NCS structure. We are in the process of synthesizing other quaternary mixed metal oxide materials and will be reporting on them shortly.

■ ASSOCIATED CONTENT

Supporting Information. X-ray crystallographic file in CIF format, calculated and observed X-ray diffraction patterns, thermogravimetric analysis diagrams, UV−vis diffuse reflectance spectra, Infrared spectra, and ORTEP drawings for $InVTe_2O_8$ and $InVSe_2O_8$. This material is available free of charge via the Internet at http://pubs.acs.org.

■ AUTHOR INFORMATION

Corresponding Author

*Tel.: +82-2-820-5197. Fax: +82-2-825-4736. E-mail: kmok@cau.ac.kr.

■ ACKNOWLEDGMENT

This research was supported by Basic Science Research Program through the National Research Foundation of Korea (NRF) funded by Ministry of Education, Science & Technology (throguh Grant No. 2010-0002480). P.S.H. thanks the Robert A. Welch Foundation (through Grant No. E-1457), the Texas Center for Superconductivity, and the NSF (No. DMR-0652150) for support.

■ REFERENCES

(1) Champarnaud-Mesjard, J. C.; Frit, B.; Chagraoui, A.; Tairi, A. *J. Solid State Chem.* **1996**, *127*, 248.
(2) Champarnaud-Mesjard, J. C.; Frit, B.; Chagraoui, A.; Tairi, A. *Z. Anorg. Allg. Chem.* **1996**, *622*, 1907.
(3) Ok, K. M.; Halasyamani, P. S. *Chem. Mater.* **2002**, *14*, 2360.
(4) Zhang, W.; Tao, X.; Zhang, C.; Gao, Z.; Zhang, Y.; Yu, W.; Cheng, X.; Liu, X.; Jiang, M. *Cryst. Growth Des.* **2008**, *8*, 307.
(5) Galy, J.; Lindqvist, O. *J. Solid State Chem.* **1979**, *27*, 279.
(6) Alonso, J. A.; Castro, A.; Puebla, E. G.; Monge, M. A.; Rasines, I.; Valero, C. R. *J. Solid State Chem.* **1987**, *69*, 36.
(7) Halasyamani, P. S.; O'Hare, D. *Chem. Mater.* **1998**, *10*, 646.
(8) Blanchandin, S.; Champarnaud-Mesjard, J. C.; Thomas, P.; Frit, B. *J. Alloys Compd.* **2000**, *306*, 175.
(9) Ok, K. M.; Zhang, L.; Halasyamani, P. S. *J. Solid State Chem.* **2003**, *175*, 264.
(10) Alcock, N. W.; Harrison, W. D. *Acta Crystallogr., Sect. B: Struct. Crystallogr. Cryst. Chem.* **1982**, *B38*, 1809.
(11) Mayer, H.; Weil, M. *Z. Anorg. Allg. Chem.* **2003**, *629*, 1068.
(12) Ok, K. M.; Orzechowski, J.; Halasyamani, P. S. *Inorg. Chem.* **2004**, *43*, 964.
(13) Kim, M. K.; Kim, S.-H.; Chang, H.-Y.; Halasyamani, P. S.; Ok, K. M. *Inorg. Chem.* **2010**, *49*, 7028.
(14) Halasyamani, P. S.; Poeppelmeier, K. R. *Chem. Mater.* **1998**, *10*, 2753.
(15) Ok, K. M.; Bhuvanesh, N. S. P.; Halasyamani, P. S. *Inorg. Chem.* **2001**, *40*, 1978.
(16) Ok, K. M.; Halasyamani, P. S. *Angew. Chem., Int. Ed.* **2004**, *43*, 5489.
(17) Kepert, C. J.; Prior, T. J.; Rosseinsky, M. J. *J. Am. Chem. Soc.* **2000**, *122*, 5158.
(18) Maggard, P. A.; Stern, C. L.; Poeppelmeier, K. R. *J. Am. Chem. Soc.* **2001**, *123*, 7742.
(19) Hwu, S.-J.; Ulutagay-Kartin, M.; Clayhold, J. A.; Mackay, R.; Wardojo, T. A.; O'Connor, C. J.; Kraweic, M. *J. Am. Chem. Soc.* **2002**, *124*, 12404.
(20) Welk, M. E.; Norquist, A. J.; Arnold, F. P.; Stern, C. L.; Poeppelmeier, K. R. *Inorg. Chem.* **2002**, *41*, 5119.
(21) Jona, F.; Shirane, G. *Ferroelectric Crystals*; Pergamon Press: Oxford, U.K., 1962.
(22) Cady, W. G. *Piezoelectricity: An Introduction to the Theory and Applications of Electromechanical Phenomena in Crystals*; Dover: New York, 1964.
(23) Lang, S. B. *Sourcebook of Pyroelectricity*; Gordon & Breach Science: London, 1974.
(24) Galy, J.; Meunier, G. *J. Solid State Chem.* **1975**, *13*, 142.
(25) Opik, U.; Pryce, M. H. L. *Proc. R. Soc. London A* **1957**, *A238*, 425.
(26) Bader, R. F. W. *Mol. Phys.* **1960**, *3*, 137.
(27) Pearson, R. G. *J. Mol. Struct.: THEOCHEM* **1983**, *103*, 25.
(28) Wheeler, R. A.; Whangbo, M.-H.; Hughbanks, T.; Hoffmann, R.; Burdett, J. K.; Albright, T. A. *J. Am. Chem. Soc.* **1986**, *108*, 2222.
(29) Goodenough, J. B. *Annu. Rev. Mater. Sci.* **1998**, *28*, 1.
(30) Orgel, L. E. *J. Chem. Soc.* **1959**, 3815.
(31) Waghmare, U. V.; Spaldin, N. A.; Kandpal, H. C.; Seshadri, R. *Phys. Rev. B* **2003**, *67*, 125111.
(32) Stoltzfus, M. W.; Woodward, P.; Seshadri, R.; Park, J.-H.; Bursten, B. *Inorg. Chem.* **2007**, *46*, 3839.
(33) Darriet, J.; Guillaume, G.; Wilhelmi, K. A.; Galy, J. *Acta Chem. Scand.* **1972**, *26*, 59.
(34) Hong, Y. S.; Darriet, J.; Yoon, J. B.; Choy, J. H. *Jpn. J. Appl. Phys., Part 1* **1999**, *38*, 1506.
(35) Harrison, W. T. A.; Buttery, J. H. N. *Z. Anorg. Allg. Chem.* **2000**, *626*, 867.
(36) Rozier, P.; Vendier, L.; Galy, J. *Acta Crystallogr., Sect. C: Cryst. Struct. Commun.* **2002**, *C58*, i111.
(37) Hou, J. Y.; Huang, C. C.; Zhang, H. H.; Yang, Q. Y.; Chen, Y. P.; Xu, J. F. *Acta Crystallogr., Sect. C: Cryst. Struct. Commun.* **2005**, *C61*, i59.
(38) Johnston, M. G.; Harrison, W. T. A. *Acta Crystallogr., Sect. C: Cryst. Struct. Commun.* **2007**, *C63*, i57.
(39) Pitzschke, D.; Jansen, M. *Z. Anorg. Allg. Chem.* **2007**, *633*, 1563.
(40) Jiang, H.; Huang, S.; Fan, Y.; Mao, J.; Cheng, W. *Chem.—Eur. J.* **2008**, *14*, 1972.
(41) Grzechnik, A.; Halasyamani, P. S.; Chang, H.; Friese, K. *J. Solid State Chem.* **2009**, *182*, 1570.
(42) Zhang, D.; Johnsson, M. *Acta Crystallogr., Sect. C: Cryst. Struct. Commun.* **2009**, *C65*, i9.
(43) Kim, Y. T.; Kim, Y. H.; Park, K.; Kwon, Y. U.; Young, V. G., Jr. *J. Solid State Chem.* **2001**, *161*, 23.
(44) Sivakumar, T.; Chang, H. Y.; Baek, J.; Halasyamani, P. S. *Chem. Mater.* **2007**, *19*, 4710.
(45) Jiang, H.; Kong, F.; Fan, Y.; Mao, J. *Inorg. Chem.* **2008**, *47*, 7430.
(46) Li, P.-X.; Zhang, S.-Y.; Mao, J.-G. *Dalton Trans.* **2010**, *39*, 11560.
(47) Zhang, S.-Y.; Hu, C.-L.; Sun, C.-F.; Mao, J.-G. *Inorg. Chem.* **2010**, *49*, 11627.
(48) SAINT, Version 4.05; Program for Area Detector Absorption Correction, Siemens Analytical X-ray Instruments, Madison, WI, 1995.
(49) Blessing, R. H. *Acta Crystallogr., Sect. A: Found. Crystallogr.* **1995**, *A51*, 33.
(50) Sheldrick, G. M. *SHELXS-97—A Program for Automatic Solution of Crystal Structures*; University of Goettingen: Goettingen, Germany, 1997.
(51) Sheldrick, G. M. *SHELXL-97—A Program for Crystal Structure Refinement*; University of Goettingen: Goettingen, Germany, 1997.
(52) Farrugia, L. J. *J. Appl. Crystallogr.* **1999**, *32*, 837.
(53) Kubelka, P.; Munk, F. *Z. Tech. Phys.* **1931**, *12*, 593.
(54) Tauc, J. *Mater. Res. Bull.* **1970**, *5*, 721.
(55) Kurtz, S. K.; Perry, T. T. *J. Appl. Phys.* **1968**, *39*, 3798.
(56) Ok, K. M.; Chi, E. O.; Halasyamani, P. S. *Chem. Soc. Rev.* **2006**, *35*, 710.

(57) Brown, I. D.; Altermatt, D. *Acta Crystallogr., Sect. B: Struct. Sci.* **1985**, *B41*, 244.
(58) Brese, N. E.; O'Keeffe, M. *Acta Crystallogr., Sect. B: Struct. Sci.* **1991**, *B47*, 192.
(59) Sivakumar, T.; Ok, K. M.; Halasyamani, P. S. *Inorg. Chem.* **2006**, *45*, 3602.
(60) Lee, D. W.; Ok, K. M. *Solid State Sci.* **2010**, *12*, 2036.
(61) Vaughey, J. T.; Harrison, W. T. A.; Dussack, L. L.; Jacobson, A. J. *Inorg. Chem.* **1994**, *33*, 4370.
(62) Frost, R. L.; Erickson, K.; Weier, M. L. *Spectrochem. Acta* **2004**, *60A*, 2419.
(63) Sullens, T. A.; Albrecht-Schmitt, T. E. *Inorg. Chem.* **2005**, *44*, 2282.
(64) Zheng, S.-T.; Zhang, J.; Yang, G.-Y. *Inorg. Chem.* **2005**, *44*, 2426.
(65) Sykora, R. E.; Ok, K. M.; Halasyamani, P. S.; Wells, D. M.; Albrecht-Schmitt, T. E. *Chem. Mater.* **2002**, *14*, 2741.
(66) Touboul, M.; Toledano, P. *Acta Crystallogr., Sect. B: Struct. Crystallogr. Cryst. Chem.* **1980**, *B36*, 240.
(67) Senegas, J.; Manaud, J. P.; Galy, J. *Acta Crystallogr., Sect. B: Struct. Crystallogr. Cryst. Chem.* **1975**, *B31*, 1614.
(68) Goodey, J.; Broussard, J.; Halasyamani, P. S. *Chem. Mater.* **2002**, *14*, 3174.
(69) Maggard, P. A.; Nault, T. S.; Stern, C. L.; Poeppelmeier, K. R. *J. Solid State Chem.* **2003**, *175*, 25.
(70) Izumi, H. K.; Kirsch, J. E.; Stern, C. L.; Poeppelmeier, K. R. *Inorg. Chem.* **2005**, *44*, 884.
(71) Kim, M. K.; Jo, V.; Lee, D. W.; Ok, K. M. *Dalton Trans.* **2010**, *39*, 6037.